6ICEGE 6th International Conference on Earthquake Geotechnical Engineering
1-4 November 2015
Christchurch, New Zealand

Tests of Permeability in Saturated Sand during Liquefaction

T. S. Ueng[1], Z.F. Wang[2], M.C. Chu[3], L. Ge [4]

ABSTRACT

For understanding and modeling the behavior of saturated sand during liquefaction, the permeability of the sand is a very important property affecting drainage, pore pressure buildup and dissipation, and ground settlement. A laboratory experiment system was developed to conduct tests for evaluating the water movements and permeability in a sand column before, during and after liquefaction. The excess pore water pressures at various depths along the sand specimen, hydraulic gradients, and water flow rates were recorded continuously during the tests. Thus, the coefficient of permeability of the sand can be determined during the process of soil liquefaction. Results showed that the permeability of fine Vietnam sand during liquefaction was about 4 times the initial value before liquefaction, while it reduced to 0.9 times the initial value after full dissipation of the excess pore pressures.

Introduction

There are two situations when the pore water pressure in sand reaches its overburden stress resulting in a state that the sand loses grain contacts and its shear strength. One is sand boiling. According to Terzaghi's effective stress concept, the soil particles begin to be lifted into suspension when the seepage force equals the initial effective stress in soil (Terzaghi et al. 1996). The critical hydraulic gradient i_{cr} required to reach the state of sand boiling can be expressed as the buoyant unit weight of soil γ' divided by the unit weight of water γ_w, i.e., $i_{cr} = \gamma' / \gamma_w$. It was found that when sand boiling occurred, the permeability of the sand increased suddenly.

The other situation is soil liquefaction due to the pore water pressure increases induced by shakings such as earthquake loading. Structures may be damaged due to concurrently the seismic loading and the loss of the soil supporting strength and ground settlements caused by soil liquefaction. Ishihara (1994) summarized the results of various predictions for VELACS model 1 and concluded that the post-liquefaction behavior of liquefied sands is significantly affected by the soil permeability. Centrifuge tests were conducted using resistivity measurement by Arulanandan and Sybico (1993) to characterize the soil structure during and after liquefaction. By applying the Kozeny–Carman equation to the test results, they found that the coefficient of permeability of the soil specimen during liquefaction increased 6 to 7 times its initial value as the pore shape factor and tortuosity decreased. It was further indicated that the predicted settlement using the initial permeability of the specimen would be

[1] Professor Emeritus, Department of Civil Engineering, National Taiwan University, Taipei, Taiwan, ueng@ntu.edu.tw
[2] Geotechnical Engineer, Civil & Building Engineering Department, CTCI Corporation, Taipei, Taiwan, purple.wang@ctci.com.tw
[3] Former graduate student, Department of Civil Engineering, National Taiwan University, Taipei, Taiwan, r02521128@ntu.edu.tw
[4] Associate Professor, Department of Civil Engineering, National Taiwan University, Taipei, Taiwan, louisge@ntu.edu.tw

underestimated. A modified consolidation theory was proposed by Scott (1986) to consider the relation between solidification velocity and permeability of saturated sand. Kim et al. (2009) combined Scott's theory with their centrifuge test results and developed a nonlinear solidification model. It was found that the solidification velocity increased with increase of particle size and relative density of the specimens. Wang et al. (2013) combined the test results of 1-g shaking table tests with the nonlinear solidification model and consolidation theory, and concluded that the post-liquefaction behavior can be predicted well by considering the changes of permeability after liquefaction.

However, previous evaluations of the changes of permeability of liquefied sand during and after liquefaction based on the assumption of drainage flow through the liquefied sand or the application of solidification and consolidation theory may not truly represent the flow conditions within the soil during and after liquefaction. A new experimental approach is proposed in this study by combining seepage and liquefaction tests to directly measure the changes of permeability of saturated sand during liquefaction which is an important parameter for evaluation of liquefaction and resulting settlement.

Testing Program

Fine Vietnam silica sand (D_r = 40.7% and dry unit weight = 14.5 kN/m^3) was used for the saturated sand specimens. The physical properties of the sand are shown in Table 1. The experimental system shown in Figure 1 includes the permeameter containing a sand specimen of 100 mm in diameter and 500 mm in length, a constant head water supply system, and a data acquisition system for continuous measurements of water pressure and flow velocity during the tests. The specimen was prepared in 10 layers by wet sedimentation method. A thin layer of colored sand was placed between the sand layers for observing the deformation of each sand layer throughout the tests. Four pressure transducers, P1, P2, P3, and P4 were installed on the wall of the permeameter. The test program summarized in Table 2 includes: (1) seepage-induced failure (sand boiling) tests; (2) liquefaction tests without seepage; and (3) liquefaction tests with seepage of various flow velocities. For the seepage-induced failure tests, the sand specimen was subjected to stepwise increased upward flow from the bottom until sand boiling occurred. Liquefaction of the sand was induced by applying a series of shocks manually using a rubber hammer. The frequency and duration of the shocks were about 4.5 Hz and 6 seconds, respectively. For liquefaction tests with seepage, a small upward flow was applied prior to application of vibrations to the sand specimen, and maintained at a constant flow velocity throughout the liquefaction test. The excess pore pressures, the flow velocity and the surface settlements were recorded during the tests. Therefore, the changes of water pressures and the seepage situations could be observed during the process of soil liquefaction. In addition, the coefficients of permeability of the sand specimen before vibration k_i and after excess pore pressure dissipation k_{end} were measured by the constant head permeability tests. The initial value of k_i was found about 5.9×10^{-2} cm/s.

Table 1. Physical properties of fine Vietnam silica sand.

Particle shape	$\mathbf{G_s}$	$\mathbf{D_{10}}$ **(mm)**	$\mathbf{D_{60}}$ **(mm)**	$\mathbf{C_u}$	$\mathbf{e_{max}}$	$\mathbf{e_{min}}$
Sub-angular	2.65	0.22	0.34	1.545	0.906	0.631

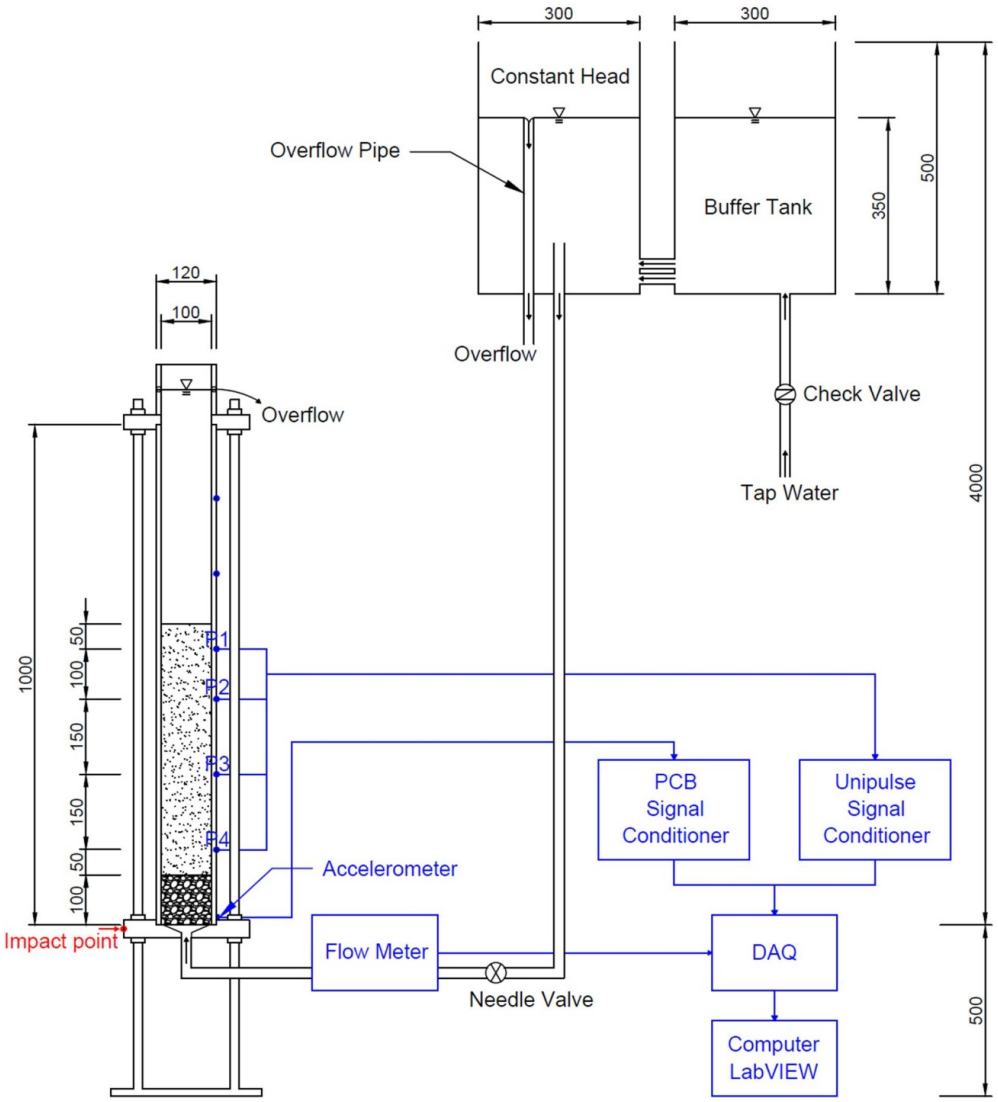

Figure 1. Schematic diagram of the experiment system (length in mm)

Table 2. Summary of testing program.

Tests	Test contents	Flow velocity, v_i (10^{-2} cm/s)
S	Seepage-induced failure (sand boiling) test	Varies
L	Liquefaction test without seepage	0
LS1	Liquefaction test with seepage	≈ 0.5
LS2	Liquefaction test with seepage	≈ 1.0
LS3	Liquefaction test with seepage	≈ 2.2

Test Results

For the analysis of the test results, the zones of the specimen between P1 and P2, P2 and P3, and P3 and P4 are defined as zone 1, zone 2, and zone 3, respectively. The thickness of zone 1, zone 2, and zone 3 are 100 mm, 150 mm, and 150 mm, respectively. In this study, the pore

water pressure changes were recorded by the 4 pressure transducers throughout the tests. The excess pore pressures exceeding the initial hydrostatic pressures at the locations of the 4 pressure transducers were expressed in terms of height of water in mm. When the excess pore pressures at the locations of P1, P2, P3, and P4 are different, the excess pore pressure head gradient is defined as:

$$i_{ej} = \frac{h_{e(j+1)} - h_{ej}}{H_j}, \quad (j = 1, 2, 3) \tag{1}$$

where i_{ej} is the excess pore pressure head gradient in zone j, h_{ej} is the excess pore pressure head at pressure transducer P_j, and H_j is the thickness of zone j. In an ordinary seepage test, i_e is equal to hydraulic gradient i, which induces the water flow. However, in the liquefaction tests of this study, the i_e generated by vibrations with or without water flow may not necessarily be the driving source of the water flow. Further discussions will be given in the later sections.

Figure 2 shows typical time histories of the excess pore pressures measured by the 4 pressure transducers in liquefaction test LS2-1 with a flow velocity of 0.98×10^{-2} cm/s. Before application of vibrations, there was an excess pore pressure gradient across the sand specimen due to the small upward water flow. Under the vibration loading, it was observed that the soil at the shallower depth was liquefied. The excess pore pressures measured by P1 and P2 in the liquefied zone maintained about the values of the initial effective stresses corresponding to the depths of P1 (50 mm) and P2 (150 mm) during liquefaction. The excess pore pressure head gradient in zone 1 during liquefaction i_{el} calculated by Equation 1 is about 0.955. On the other hand, the increase rate of excess pore pressures in the non-liquefied zone measured by P3 and P4 began to decrease shortly after the time of liquefaction of the shallower layer. It was inferred that the dissipation of the excess pore pressure in the non-liquefied zone during vibration was affected by the change of permeability in the liquefied zone. Fast dissipations of the excess pore pressures measured in both liquefied and non-liquefied zones were observed when the vibration stopped.

The similar trend of time histories of the excess pore pressures in both liquefied and non-liquefied zones was observed in other liquefaction tests in this study with different flow velocities. The average excess pore pressure head gradients in zone 1 during liquefaction i_{el} calculated by Equation 1 are 0.917, 0.940, 0.955, and 1.0 for tests L, LS1, LS2, and LS3, respectively.

In addition, the observed changes of the locations of the colored sands and the surface of the sand specimen showed that the settlement of the sand column in the liquefaction tests occurred at the beginning of vibration, continued during the process of vibration, and ceased about the time when vibration stopped. Similar to the findings by Ueng et al. (2010), significant settlement was induced only when liquefaction occurred, while almost no settlement was observed in the non-liquefied zone after liquefaction tests. The settlements S_l of the liquefied zones in test L, LS1, LS2, and LS3 were approximately 3 mm, 2.5 mm, 2.5 mm, and 2 mm, respectively. S_l decreased with increasing upward flow velocity probably because the upward flow may hinder the sand particles from sedimentation after liquefaction.

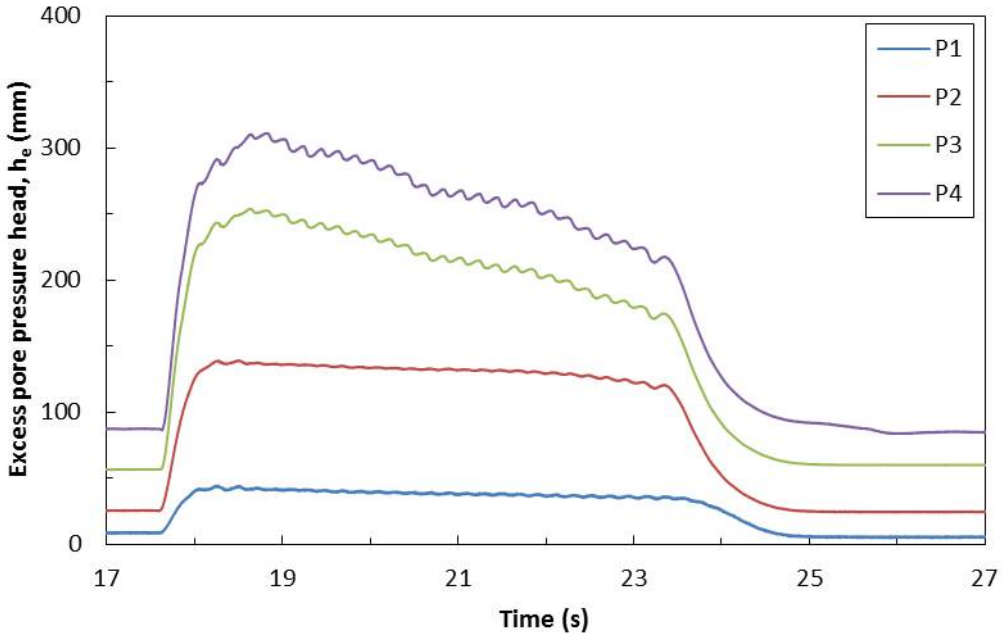

Figure 2. Time history of excess pore pressures in test LS2-1

Permeability of Liquefied Sand

According to the liquefaction test results, the value of i_{el} increased with increasing upward flow velocity. In this study, an effective hydraulic gradient in zone 1 during liquefaction i_l is defined as the net source that drives the upward water flow through the liquefied zone during liquefaction, and can be expressed as:

$$i_l = i_{el,LS} - i_{el,L} \tag{2}$$

where $i_{el,LS}$ and $i_{el,L}$ are the excess pore pressure head gradients during liquefaction in tests with and without seepage (tests LS and L), respectively. Under the assumption of the applicability of Darcy's law, the coefficient of permeability of the liquefied sand during liquefaction k_l can be calculated from the measured flow velocity during liquefaction v_l divided by the effective hydraulic gradient in zone 1 during liquefaction i_l, i.e.,

$$k_l = v_l / i_l \tag{3}$$

Figure 2 shows a linear relation between i_{el} and v_l obtained in the liquefaction tests of this study. The k_l can then be calculated by combining Equations 2 and 3 or directly obtained from the inverse slope of the linear relation in Figure 3. The value of k_l thus obtained in the liquefaction tests with different water flow velocities was 25.6×10^{-2} cm/s, about 4 times the initial values, i.e., $k_l / k_i \approx 4$. This linear relation in Figure 3 also indicates that the small upward water flow applied in this study did not significantly affect the changes of soil conditions during liquefaction. On the other hand, the coefficients of permeability after full dissipation of the excess pore pressure in the liquefaction test series LS were about 0.9 times the initial values. This can be attributed to the decrease in the void ratio of the sand specimen after full dissipation of excess pore pressure.

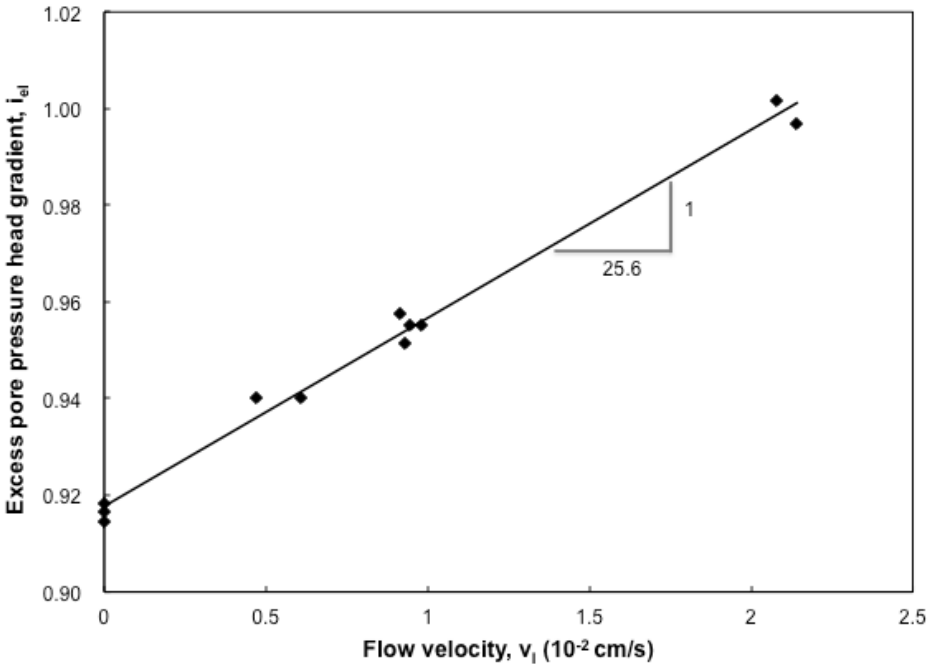

Figure 3. Excess pore pressure gradient versus flow velocity within liquefied sand

Discussions

The increase of the permeability of the liquefied sand during liquefaction can be interpreted by applying Kozeny–Carman equation for the permeability of saturated porous media (Kozeny 1927, Carman 1956), i.e.,

$$k = \left(\frac{1}{k_0 T}\right)\left(\frac{\gamma_p}{\mu}\right)\frac{1}{S_0^{\,2}}\left(\frac{e^3}{1+e}\right) \tag{4}$$

where k is the coefficient of permeability of the porous media, k_0 is the pore shape factor, T is the tortuosity factor, γ_p is the unit weight of the flowing fluid, μ is the viscosity of the flowing fluid, S_0 is the wetted surface area per unit volume of particles, and e is the void ratio of the porous media. A simplified representation of the tortuosity factor T can be expressed as the mean length of the flow path of the fluid through the porous media L divided by the distance between the ends of the porous media C, i.e., T = L/C. Figure 4 shows the schematic diagram of water flow through the sand at initial and liquefied states. At the initial state, the sand particles are contact with each other. The water flow cannot pass through the contact points in the sand specimen. Thus, the flow path of the water through the sand specimen L is much longer than the length of the sand specimen C. During liquefaction of the sand, the sand particles lose their contacts, and water can more directly flow through the sand specimen without bypassing the grain contacts resulting in a shorter path for water to flow through the liquefied sand. Therefore, the coefficient of permeability of the sand specimen during liquefaction increases as the tortuosity of the sand specimen decreases; while it is assumed that the change in the void ratio of the liquefied sand during liquefaction was negligible.

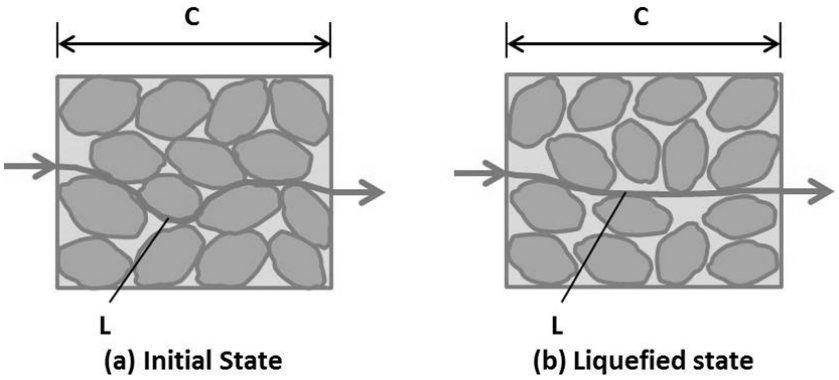

Figure 4. Schematic diagram of water flow through sand specimen at different states

Conclusions

In this study, a new experimental approach was proposed by combining the seepage test with the liquefaction test to directly evaluate the variation of permeability of saturated sand before, during and after liquefaction. During liquefaction, the permeability of the liquefied sand was found to be about 4 times the initial value before liquefaction and it reduced to about 0.9 of the initial value after full dissipation of the excess pore pressure and complete settlement of the sand specimen. The sand particles lose their contacts at liquefaction, which create an easier path for water to flow through the liquefied sand. The coefficient of permeability of the sand specimen increases as the tortuosity of the sand specimen decreases during liquefaction.

References

Arulanandan K, Sybico, Jr. J. *Post-liquefaction settlement of sand. Proceedings of the Wroth memorial symposium.* Oxford University: England, 1992; 94-110.

Carman PC. *Flow of Gases through Porous Media.* Academic: New York, 1956.

Ishihara K. Review of the predictions for Model 1 in the VELACS program. Arulanandan, K., Scott, R.F., editors, *Verification of numerical procedures for the analysis of soil liquefaction problems.* Balkema, A. A.: Rotterdam, 1994; 1353–1368.

Kim SR, Hwang JI, Ko HY, Kim MM. Development of dissipation model of excess pore pressure in liquefied sandy ground. *Journal of Geotechnical and Geoenvironmental Engineering,* ASCE 2009; **135** (4): 544-554.

Kozeny J. *Ueber kapillare Leitung des Wassers im Boden.* Wien, Akad. Wiss 1927; **136** (2a): 271.

Scott RF. Solidification and consolidation of a liquefied sand column. *Soils and Foundations* 1986; **26** (4): 23-31.

Terzaghi K, Peck RB, Mesri G. *Soil Mechanics in Engineering Practice.* 3rd edition, John Wiley & Sons: New York, 1996.

Ueng TS, Wu CW, Cheng HW, Chen CH. Settlement of saturated clean sand deposits in shaking table tests. *Soil Dynamics and Earthquake Engineering* 2010; **30** (1): 50-60.

Wang B, Zen K, Chen GQ, Zhang YB, Kasama K. Excess pore pressure dissipation and solidification after liquefaction of saturated sand deposits. *Soil Dynamics and Earthquake Engineering* 2013; **49**: 157-164.